Hum. Reprod. Advance Access published May 2, 2011
Human Reproduction, Vol.0, No.0 pp. 1–9, 2011
doi:10.1093/humrep/der129

human reproduction

ORIGINAL ARTICLE *Andrology*

Large human sperm vacuoles observed in motile spermatozoa under high magnification: nuclear thumbprints linked to failure of chromatin condensation

F. Boitrelle[1,2,*], F. Ferfouri[1,2], J.M. Petit[3], D. Segretain[3], C. Tourain[3], M. Bergere[1,2], M. Bailly[1], F. Vialard[1,2], M. Albert[1,2], and J. Selva[1,2]

[1]Department of Reproductive biology, Cytogenetics and Gynecology, Hospital of Poissy, CHIPS, Poissy 78303, France [2]EA 2493, University of Medicine and Science, Versailles-Saint-Quentin en Yvelines 78000, France [3]Department of Microscopy SCM, University of Medicine and Science, Paris V 75006, France

*Correspondence address. Tel: +33-1-39-27-47-00; Fax: +33-1-39-27-44-25; E-mail: florenceboitrelle@yahoo.fr

Submitted on February 2, 2011; resubmitted on March 21, 2011; accepted on March 29, 2011

BACKGROUND: An embryo's ability to grow and implant can be improved by selection of a normal spermatozoon with a vacuole-free head. However, large vacuoles in spermatozoa have yet to be fully characterized. The present study aimed to determine whether these vacuoles are of nuclear, membrane and/or acrosomal origin.

METHODS: We studied 15 infertile patients with differing sperm profiles. For each sperm sample, we used high-magnification (×10 000) contrast microscopy to select and assess 30 normal 'top' spermatozoa and 30 spermatozoa with a large sperm-head vacuole (≥ 25% of the head's cross-sectional area). We subsequently analysed the spermatozoa's degree of chromatin condensation (aniline blue staining), DNA fragmentation (terminal deoxyribonucleotidyl transferase-mediated dUTP nick-end labelling assay) and chromosome content (fluorescence *in situ* hybridization X,Y,18). Atomic force microscopy enabled us to map the plasma sperm membrane in detail. Three-dimensional deconvolution microscopy enabled us to reconstruct images of the nucleus and acrosome in 'top' and 'vacuolated' spermatozoa.

RESULTS: We studied a total of 450 'top' spermatozoa and 450 vacuolated spermatozoa. The rate of non-condensed chromatin was higher for 'vacuolated' spermatozoa than for 'top' spermatozoa (36.2 ± 1.9 versus 7.6 ± 1.3%, respectively; $P < 0.0001$). 'Top' and 'vacuolated' spermatozoa did not differ significantly in terms of DNA fragmentation (0.7 ± 0.4 versus 1.3 ± 0.4% respectively; $P = 0.25$) or aneuploidy (1.1 ± 0.5 versus 2.2 ± 0.7% respectively; $P = 0.21$). The majority of aneuploid spermatozoa (9 out of 15) lacked chromatin condensation. In all vacuolated spermatozoa, the acrosome was intact, the plasma membrane was sunken but intact and the large vacuole was identified as an abnormal, 'thumbprint'-like nuclear concavity covered by acrosomal and plasmic membranes.

CONCLUSIONS: The large vacuole appears to be a nuclear 'thumbprint' linked to failure of chromatin condensation.

Key words: large sperm-head vacuole / sperm chromatin condensation / nuclear thumbprint / 3D deconvolution microscopy / epigenetic markers

Introduction

Since 1992, ICSI has enabled many infertile men to become biological fathers (Palermo *et al.*, 1992). However, the quality of the sperm used may affect post-ICSI fertilization and cleavage rates, embryo quality (Loutradi *et al.*, 2006) and implantation and pregnancy rates (De Vos *et al.*, 2003). Since 2002, motile sperm organellar morphology examination (MSOME) under high magnification [×6600 with Nomarski/differential interference contrast (DIC)] has been used to select 'top' spermatozoa that may be of higher quality (Bartoov *et al.*, 2002, 2003). In fact, MSOME has shown that some spermatozoa, which appear morphologically normal when viewed at ×400 or ×200, present defects such as cephalic vacuoles when viewed under high magnification (Bartoov *et al.*, 2002). Selection of a 'top' spermatozoon with MSOME prior to intracytoplasmic injection (IMSI) is associated with higher blastocyst, implantation and pregnancy rates

and lower miscarriage rates. A 'top' spermatozoon is defined as having a morphologically and morphometrically normal head (Bartoov et al., 2002, 2003; Berkovitz et al., 2005; Hazout et al., 2006; Antinori et al., 2008) with no vacuoles (Berkovitz et al., 2006) or fewer than two small vacuoles (Cassuto et al., 2009) that account for less than 4% of the head's cross-sectional area (Vanderzwalmen et al., 2008). However, the nature of these vacuoles is unknown and so the value of MSOME in selecting high-quality spermatozoa is still subject to debate. To improve the criteria for selection of 'top' spermatozoa, it is important to characterize these sperm-head vacuoles.

In the late stages of spermatogenesis, spermatid maturation (spermiogenesis) has been defined as the sum of a series of complex, and sometimes epigenetic, events involved in chromatin condensation, acrosome and tail genesis, cytoplasm extrusion and the biochemical remodelling of the sperm plasma membrane. Abnormalities in these various steps could lead to functional deficiencies, such as the failure of chromatin condensation, susceptibility to DNA damage, the presence of an abnormally small acrosome or immaturity of the sperm plasma membrane. However, the methods currently used to evaluate these sperm quality criteria are invasive and involve the use of fluorescent probes and/or the fixation of spermatozoa—thus preventing their subsequent injection into oocytes. Recently, a few authors have reported relationships between the presence of a large sperm-head vacuole and failure of chromatin condensation (Garolla et al., 2008; Perdrix et al., 2011) and/or DNA damage (Franco et al., 2008; Garolla et al., 2008) and/or aberrant chromosome numbers in spermatozoa (Garolla et al., 2008; Perdrix et al., 2011). But the nature of vacuoles remains unclear. These various vacuoles can be small or large, anterior or posterior and deep-lying or superficial and may not all have the same origin. Thus, to establish a relationship between one type of vacuole morphology and nuclear status, we used MSOME to select 'top' spermatozoa and spermatozoa with a large vacuole but otherwise normal. We then compared the spermatozoon's nuclear status by analysing chromatin condensation, DNA fragmentation and chromosome content, with 900 spermatozoa analysed.

Furthermore, we used atomic force microscopy (AFM) to (i) evaluate potentially abnormal remodelling, (ii) analyse the integrity, shape and ultra-fine appearance of a plasma membrane, (iii) measure the spermatozoon's size in all three dimensions and (iv) determine whether the vacuole was part of the sperm plasma membrane. Since AFM is a time-consuming technique (about 4 h per spermatozoon, including selection), a total of 40 spermatozoa (from two patients) were analysed.

It has recently been suggested that injection of the acrosome into the oocyte could be harmful for embryo development (Morozumi and Yanagimachi, 2005). So, it would be interesting to link the morphology of motile sperm, and in particular the absence or presence of a large vacuole, to the acrosomal status, as proposed recently (Kacem et al., 2010). In order to better define the structures involved in the large vacuoles, we used, for the first time here, a more original imaging approach: the three-dimensional (3D) deconvolution microscopy. This novel tool for visualizing structures in 3D (Biggs, 2010) was used to reconstruct precise images of the acrosome and the nucleus in a total of 200 'top' and 'vacuolated' spermatozoa from five patients.

Materials and Methods

The study population comprised 15 infertile men (with a normal karyotype and a variety of sperm profiles) attending the Assisted Reproductive Technologies Centre at Poissy General Hospital (Poissy, France). The subjects were selected between January 2010 and April 2010. On the basis of the World Health Organization criteria (WHO, 2009) and Kruger's sperm morphology classification (Kruger et al., 1987), normal sperm characteristics were defined as follows: concentration: $>15 \times 10^6$/ml; total motility (progressive and non-progressive) >40%; progressive motility >32%. Teratozoospermia was defined as <15% of normal spermatozoa. With these criteria, five patients presented normal sperm parameters, five displayed oligoasthenoteratozoospermia and five had isolated teratozoospermia (Table I). The aetiologies of infertility were idiopathic ($n = 2$), male ($n = 2$), female ($n = 3$) or both male and female ($n = 8$).

Semen preparation, sperm selection under high magnification and nuclear status evaluation (the triple-probe procedure)

Liquefied, fresh semen samples were evaluated according to the WHO guidelines (World Health Organization, 2009) and prepared on a two-layer discontinuous concentration gradient (PureSperm 100, Nidacon, Sweden) as described previously (Frainais et al., 2010). In a glass-bottomed dish (Willco-dish, Willco wells BV, The Netherlands), 5–10 μl of the sperm fraction obtained after density-gradient selection was placed near to a 5 μl droplet of Spermslow reagent (Medicult, Denmark). The droplets were drawn together with a needle and sterile paraffin oil was added. Spermslow-bound motile spermatozoa were observed at a magnification of over ×10 000 (×100 and ×10 microscope magnification and video magnification) at room temperature with an inverted microscope (a Nikon Eclipse 2000-U, equipped with DIC optics and a ×100 dry objective lens). For each patient, two types of motile spermatozoa were selected by the same trained operator (Fig. 1), as follows:

'Top' spermatozoa ($n = 30$), which are motile and normal according to the WHO criteria (WHO, 2009), with, in particular, a normal head in shape and size. The head was symmetrical, oval regular and smooth, and presented no vacuole. Head size was normal on both axes with length and width between 4–5 and 3–3.2 μm, respectively.

'Vacuolated' spermatozoa ($n = 30$), which differed from 'top' spermatozoa only by the presence of a large vacuole in the sperm head (accounting for more than 25% of the head's cross-sectional area).

Spermatozoa were selected individually, placed in a 2 μl drop of distilled water on a glass slide as described previously (Chelli et al., 2010) and then fixed with 95% ethanol for 5 min. For each of the 15 subjects, 5 μl of the sperm fraction obtained after density-gradient selection was spread on a slide and fixed in the same way as selected spermatozoa. All slides were, then, examined with a successive triple-probe procedure. The triple-probe procedure consisted on three different staining methods after each other on the same sperm: aniline blue staining, terminal deoxyribonucleotidyl transferase-mediated dUTP nick-end labelling (TUNEL assay) and fluorescence *in situ* hybridization (FISH) assays for chromosomes X, Y and 18. Our team had already performed this procedure on spermatozoa from 20 patients (unpublished data), in order to evaluate several nuclear characteristics of the same spermatozoa. The triple-probe procedure is time-consuming (2 days per slide) and can be performed only in this order because the SDS used during the TUNEL assay and the FISH denaturation steps induces chromatin decondensation.

To evaluate sperm chromatin condensation, slides were stained with 5% acetified aniline blue (Farmitalia Carlo Erba, Italy) for 5 min, washed twice with distilled water, air dried and observed using a Metafer slide scanning platform equipped with a transmitted light microscope. As described

Table I Sperm characteristics for the 15 study subjects.

Patients (*n*)	Sperm concentration (10^6/ml)	Motility (%PR/%NP)	Normal sperm rate (%)	Classification
5	79 ± 13.6	43 ± 1/8 ± 1	25 ± 3	Normal
5	10 ± 0.5	24 ± 1/13 ± 3	6 ± 2	Oligoasthenoteratozoospermia
5	52 ± 9	42 ± 3/11 ± 1	7 ± 2	Teratozoospermia

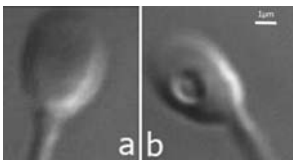

Figure 1 Spermatozoa observed under high-magnification (× 10 000) light microscopy with Nomarski contrast. (**a**) A 'top' spermatozoon; (**b**) an otherwise normal spermatozoon with a large vacuole (≥25% of the head's cross-sectional area).

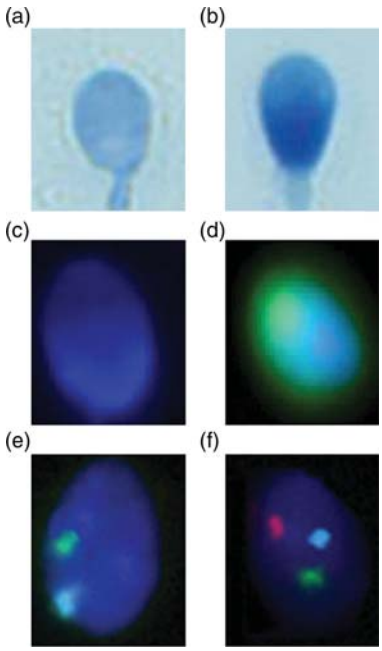

Figure 2 The triple-probe procedure. (**a**) A normally condensed chromatin spermatozoon (not stained with aniline blue); (**b**) a non-condensed chromatin spermatozoon (stained with aniline blue); (**c**) a spermatozoon with intact DNA (DAPI+/FITC−); (**d**) a DNA-fragmented spermatozoon (DAPI+/FITC+). (**e** and **f**) Examples of FISH spots in sperm nuclei. The spots for chromosomes X, Y and 18 are green, red and blue, respectively. (**e**) A euploid spermatozoon; (**f**) an aneuploid spermatozoon.

previously (Auger *et al.*, 1990), normally condensed chromatin is not stained by aniline blue (Fig. 2a). When more than 50% of the nucleus was stained (i.e. dark blue), the chromatin was considered to be non-condensed (Fig. 2b). When between 20 and 50% of the nucleus aniline-blue-stained, the chromatin was considered to be partially non-condensed. In normal sperm samples, less than 20% of chromatin is non-condensed (Auger *et al.*, 1990). For each patient, the proportion of spermatozoa with non-condensed chromatin was determined for (i) 500 spermatozoa from the fraction obtained after density-gradient selection, (ii) 30 'top' spermatozoa and (iii) 30 vacuolated spermatozoa. The sperm fields and the X/Y microscope coordinates of each spermatozoon were recorded using Metafer IV software. Aniline blue was then removed by immersion of the slides in a methanol/acetic acid (3:1) solution.

Secondly, a TUNEL kit (the Cell Death Detection kit from Roche Diagnostics, Germany) was used to assay for sperm DNA fragmentation, as described previously (Frainais *et al.*, 2010). Slides were counterstained with 4′,6-diamino-2-phenylindole (DAPI). Each previously localized spermatozoon was relocalized on the Metafer platform and observed under fluorescence conditions with using DAPI/FITC filters. Spermatozoa with a blue nucleus (DAPI+/FITC−) were classified as non-DNA-fragmented (Fig. 2c). Those with a blue and green (DAPI+/FITC+) nucleus were classified as DNA-fragmented (Fig. 2d). In our laboratory, normal sperm samples contained less than 13% of DNA-fragmented spermatozoa (Frainais *et al.*, 2010). After the TUNEL assay, slides were destained with phosphate-buffered saline (PBS) at 37°C for 30 min.

Thirdly and lastly, the sperm's aneuploidy rate was evaluated by FISH with centromere probes for chromosomes X, Y and 18 (the Aneuvysion-DNA Probe kit from Abbott, Germany), as described previously (Vialard *et al.*, 2008). Spermatozoa were observed under fluorescent light and relocalized by the Metafer platform. Interpretation criteria were based on the number of spots for chromosomes X, Y and 18 in each sperm nucleus (Fig. 2). Normal sperm samples contain less than 1% of aneuploid spermatozoa (Shi and Martin, 2001; Vialard *et al.*, 2008).

Evaluation of the sperm plasma membrane with AFM

AFM is a very high-resolution kind of scanning microscopy that provides resolution on the order of 1 nm thanks to a metallic probe which measures and records forces between it and the sperm surface. As noted above, the time-consuming nature of the AFM procedure means that it was used for one normozoospermic subject and one oligoasthenoteratozoospermic subject. For each subject, 10 'top' and 10 'vacuolated' spermatozoa were selected under high magnification and placed individually in a 2 µl drop of IVF medium (Universal IVF Medium, Medicult, Denmark) on an ultrafine glass slide. IVF medium was chosen because other media (such as distilled water, for example) can alter the sperm plasma membrane. Once the spermatozoa were passively adsorbed and immobilized, slides were immersed in IVF medium and examined under an inverted microscope equipped with an AFM unit and a vibration-free table. The spermatozoa's surface topography (Fig. 3c and f) and length, width and thickness (Fig. 3b and e) were measured simultaneously with Image J and Volume J image processing software (version 1.42, National Institutes of Health) (Fig. 3). For each spermatozoon, 10 measurements

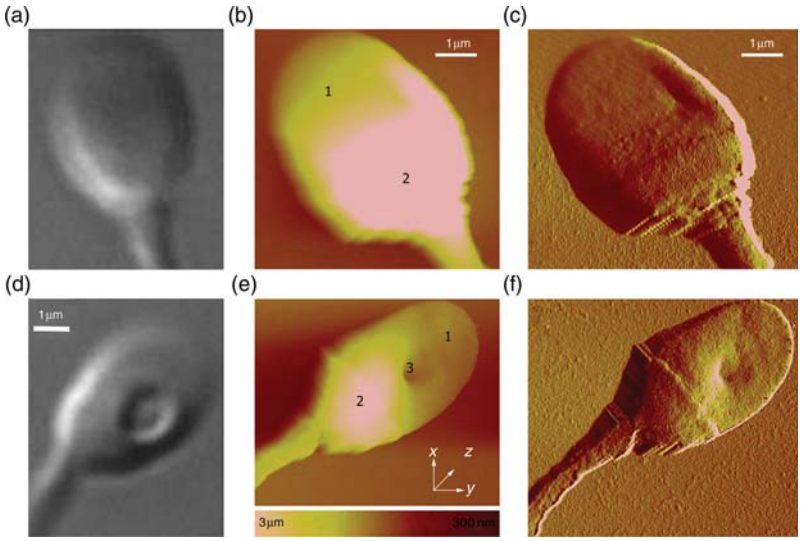

Figure 3 AFM images. (**a**) A 'top' spermatozoon observed under high-magnification (×10 000) light microscopy with Nomarski contrast; (**b**) the same 'top' spermatozoon observed using AFM, with a *z*-colour scale indicating the thickness profiles of the head region; (**c**) the same 'top' spermatozoon using AFM, with a scale bar to measure the length and width; (**d**) a 'vacuolated' spermatozoon observed under high-magnification (×10 000) light microscopy with Nomarski contrast; (**e**) the same 'vacuolated' spermatozoon observed using AFM, with a *z*-colour scale indicating the height profiles of the head region; (**f**) the same 'vacuolated' spermatozoon using AFM with a scale bar to measure the length and width.

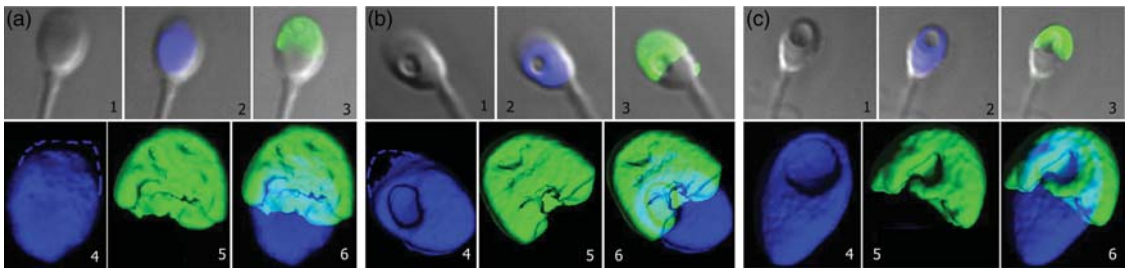

Figure 4 Three-dimensional deconvolution microscopy images. (**a**) A 'top' spermatozoon and (**b** and **c**) two 'vacuolated' spermatozoa, each observed under high magnification with Nomarski contrast (DIC) (1), a DIC/DAPI merge (2) and a DIC/FITC-labelled PSA lectin merge (3). (4–6) Three-dimensional reconstructed images of the same spermatozoa. DAPI fluoresces blue (4) and PSA lectin fluoresces green (5). Colocalization of fluorescent probes (6).

enabled us to determine the mean cross-sectional area of the anterior part of the head (1), the posterior part of the head (2) and the large vacuole (3) (Fig. 3b and e).

Evaluation of nuclear and acrosomal morphology: 3D deconvolution microscopy

Three-dimensional deconvolution microscopy is also a time-consuming technique and thus was used for only 5 of the 15 subjects (2 normozoospermic subjects, 2 oligoasthenoteratozoospermic subjects and 1 subject with isolated teratozoospermia). For each subject, 20 'top' spermatozoa and 20 'vacuolated' spermatozoa were selected under high magnification and placed individually in a 2 µl drop of IVF medium. The slides were immersed in 95% ethanol at 4°C (30 min) to permeabilize the membranes and 20 µl of 1/100 diluted *Pisum sativum* agglutinin (PSA) lectin (Sigma Aldrich, USA) was added. Next, the slides were washed with PBS (2× 3 min), air-dried and counterstained with DAPI. Simultaneous DIC/epifluorescence observations of each spermatozoon were then made with a Nikon TE2000-E microscope. Acrosome status was assessed by PSA lectin staining, according to the manufacturer's instructions: homogeneous fluorescence of the anterior region of the sperm head indicated that the acrosomal membrane and the acrosome were intact. Non-intact acrosomes are not labelled by lectin, which forms a narrow belt at the site of acrosomal membrane insertion. DAPI staining was used to label DNA and characterize the nucleus's surroundings and morphology. Each spermatozoon's cross-section was measured every 150 nm, yielding a stack of at least 25 optic sections. Image J and Volume J software were then used to produce a 3D image from the stack (Fig. 4).

Statistical analysis

Data were expressed as the mean ± standard error of the mean (SEM). Statistical analyses were performed with SAS software (version 9.1, SAS

Institute Inc., Cary, NC, USA). A Wilcoxon sum of ranks test was used to compare sperm fraction obtained after density-gradient selection, 'top' spermatozoa and 'vacuolated' spermatozoa in terms of chromatin condensation, DNA fragmentation and aneuploidy rates. The threshold for statistical significance was set to $P < 0.05$.

Results

Nuclear status

For each patient, the non-condensed chromatin rate was significantly lower for 'top' spermatozoa than for 'vacuolated' spermatozoa [7.6 ± 1.3 versus 36.2 ± 1.9%, respectively; $P = 0.000003$ (noted as $P < 0.0001$)]. Likewise, the partially non-condensed chromatin rate was significantly lower for 'top' spermatozoa than for 'vacuolated' spermatozoa (4.7 ± 1 versus 26.9 ± 2.6%, respectively; $P = 0.0000053$).

For spermatozoa obtained after density-gradient selection but not selected under high magnification, the non-condensed rate was significantly higher than for 'top' spermatozoa [25.1 ± 3.7 versus 7.6 ± 1.3%, respectively; $P = 0.000099$ (noted as $P < 0.0001$)] but lower than for 'vacuolated' spermatozoa [25.1 ± 3.7 versus 36.2 ± 1.9%, respectively; $P = 0.0096$ (noted as $P < 0.01$)] (Table II and Fig. 5).

Table II Non-condensed chromatin sperm rates for spermatozoa obtained after density-gradient selection, the 'top' spermatozoa and the 'vacuolated' spermatozoa as a function of sperm quality.

Sperm characteristics	Non-condensed chromatin sperm rates in various types of sperm, mean (%) ± SEM		
	Migrated sperm suspension (unselected spermatozoa)	'Top' spermatozoa	'Vacuolated' spermatozoa
Normal ($n = 5$ patients)	18.4 ± 3.2	6 ± 1.6[a]	35.9 ± 1.3[a]
Oligoasthenoteratozoospermia ($n = 5$ patients)	25.6 ± 6.1	7.3 ± 1.9[a]	33.3 ± 3.2[a]
Teratozoospermia ($n = 5$ patients)	35.3 ± 10.2	9.3 ± 3.1[a]	39.3 ± 4.7[a]
Total ($n = 15$ patients)	25.1 ± 3.7[c,d]	7.6 ± 1.3[b,c]	36.2 ± 1.9[b,d]

SEM, standard error of the mean. The *P*-values in a comparison of non-condensed chromatin sperm rates (Wilcoxon's sum of ranks test) are denoted as follows: [a]$P = 0.01$; [b]$P = 0.000003$; [c]$P = 0.000099$; [d]$P = 0.0096$.

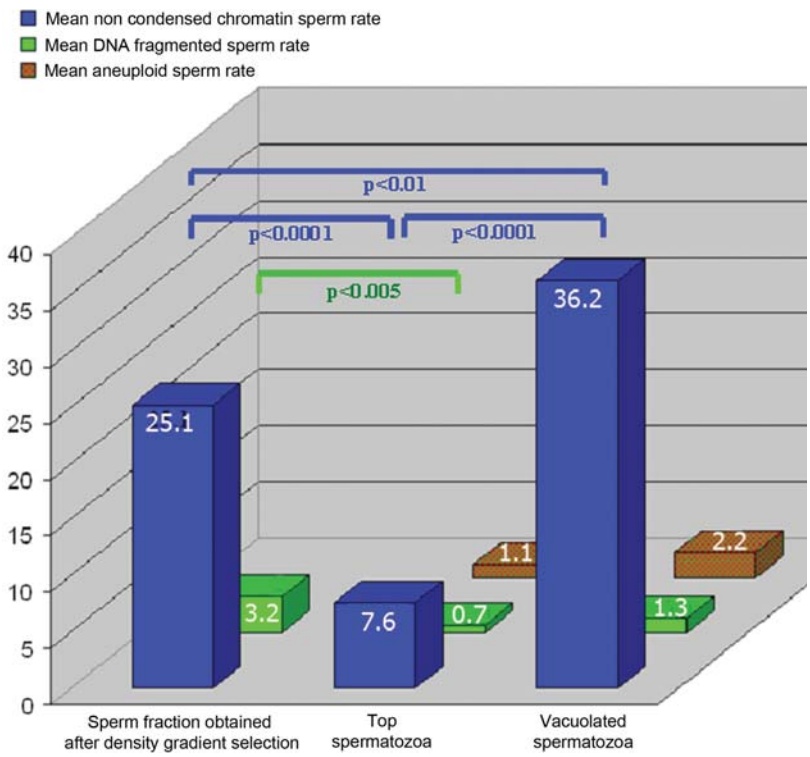

Figure 5 The non-condensed chromatin sperm rate, DNA-fragmented sperm rate and aneuploid rate for spermatozoa obtained after density-gradient selection, the 450 'top' spermatozoa and the 450 'vacuolated' spermatozoa (*P*-value in a Wilcoxon sum of ranks test).

Table III DNA fragmentation rates for spermatozoa obtained after density-gradient selection, the 'top' spermatozoa and the 'vacuolated' spermatozoa as a function of sperm quality.

Sperm characteristics	DNA-fragmented sperm rates in various types of sperm, mean (%) ± SEM		
	Migrated sperm suspension (unselected spermatozoa)	'Top' spermatozoa	'Vacuolated' spermatozoa
Normal sperm ($n = 5$ patients)	0.8 ± 0.1	0.7 ± 0.7[a]	1.3 ± 0.8[a]
Oligoasthenoteratozoospermia ($n = 5$ patients)	1.8 ± 0.6	0 ± 0[b]	0.7 ± 0.7[b]
Teratozoospermia ($n = 5$ patients)	9.3 ± 4.6	1.3 ± 0.8[c]	2 ± 0.8[c]
Total ($n = 15$ patients)	3.1 ± 1.4[e,f]	0.7 ± 0.4[d,e]	1.3 ± 0.4[d,f]

SEM, standard error of the mean. The *P*-values in a comparison of non-condensed chromatin sperm rates (Wilcoxon's sum of ranks test) are denoted as follows: [a]$P = 0.6$; [b]$P = 0.42$; [c]$P = 0.63$; [d]$P = 0.25$; [e]$P = 0.0012$; [f]$P = 0.079$.

Table IV Aneuploid sperm rates for the 'top' spermatozoa and 'vacuolated' spermatozoa as a function of sperm quality.

Sperm characteristics	Aneuploid sperm rates in various types of sperm, mean (%) ± SEM	
	'Top' spermatozoa	'Vacuolated' spermatozoa
Normal sperm ($n = 5$ patients)	1.3 ± 0.8[a]	2.7 ± 1.3[a]
Oligoasthenoteratozoospermia ($n = 5$ patients)	0.7 ± 0.7[b]	1.3 ± 1.3[b]
Teratozoospermia ($n = 5$ patients)	1.3 ± 1.3[c]	2.7 ± 1.3[c]
Total ($n = 15$ patients)	1.1 ± 0.5[d]	2.2 ± 0.7[d]

SEM, standard error of the mean. The *P*-values in a comparison of non-condensed chromatin rates (Wilcoxon's sum of ranks test) were denoted as follows: [a]$P = 0.49$; [b]$P = 1$; [c]$P = 0.4$; [d]$P = 0.21$.

'Top' and 'vacuolated' spermatozoa did not differ significantly in terms of the DNA fragmentation rate (0.7 ± 0.4 versus 1.3 ± 0.4%; $P = 0.25$). For spermatozoa obtained after density-gradient selection but not selected under high magnification, the DNA-fragmented sperm rate was statistically higher than for 'top' spermatozoa [3.1 ± 1.4 versus 0.7 ± 0.4%, respectively; $P = 0.0012$ (noted as $P < 0.005$)] but did not differ significantly from the rate for 'vacuolated' spermatozoa (3.1 ± 1.4 versus 1.3 ± 0.4%, respectively; $P = 0.079$). The DNA fragmentation rate did not appear to be correlated with the sperm parameters (Table III and Fig. 5).

Furthermore, 'top' and 'vacuolated' spermatozoa did not differ significantly in terms of aneuploidy rates [1.1 ± 0.5 ($n = 5/449$) versus 2.2 ± 0.7% ($n = 10/448$), respectively; $P = 0.21$]. The sperm parameters also did not influence the aneuploidy results (Table IV and Fig. 5). The majority of aneuploidies were disomic for gonosomes: XY18 ($n = 7$); YY18 ($n = 2$); XX18 ($n = 3$). Others were nullosomic for gonosomes ($n = 2$) or for chromosome 18 ($n = 1$). Three of the 900 spermatozoa were not analysable by FISH because the chromatin was not condensed.

Of the 205 spermatozoa with nuclear abnormalities, 189 (92.2%) had one nuclear abnormality [non-condensed chromatin ($n = 184$), DNA fragmentation ($n = 2$) or aneuploid content ($n = 3$)] and 16 (7.8%) had two nuclear abnormalities [non-condensed chromatin and DNA fragmentation ($n = 4$), non-condensed chromatin and aneuploidy ($n = 9$) or DNA fragmentation and aneuploidy ($n = 3$)]. None of the spermatozoa had three abnormalities. There was no association between chromatin condensation and DNA fragmentation or between DNA fragmentation and aneuploid spermatozoa. However, chromatin condensation had failed in the majority of aneuploid spermatozoa ($n = 9$ out of 15).

The sperm plasma membrane

The AFM images were homogeneous for all spermatozoa observed.

The 20 'top' spermatozoa had smooth, homogeneous, regular and non-sunken head surfaces (Fig. 3b and c). For each 'top' spermatozoon, our *z*-colorimetric scale showed that the head was narrower (700 nm) in the anterior region (Fig. 3b-1) than in the posterior region (3.1 μm) (Fig. 3b-2).

For all the 20 'vacuolated' spermatozoa, the sperm-head surface was sunken and the sperm plasma membrane was invaginated nearby the vacuole. The sperm plasma membrane was intact and had no extrusions. In vacuolated spermatozoa, the overall thicknesses of the anterior half of the head (Fig. 3e-1) and the posterior half of the head (Fig. 3e-2) (700 and 3 μm, respectively) did not differ significantly from the values measured for 'top' spermatozoa. However, the sperm-head's thickness fell to 300 nm at the site of the large vacuole (Fig. 3b-3), which corresponded to a concavity in the plasma membrane (Fig. 3e and f).

Nuclear and acrosomal morphology

The 3D reconstructed images were homogeneous for all spermatozoa observed. In all 100 'top' spermatozoa, the nucleus was convex and all areas contained DNA. The anterior half of the head was covered by the acrosomal membrane. The acrosomal reaction had not occurred

since the acrosomal membrane and the acrosome were intact in all cases (Fig. 4a).

For the 100 'vacuolated' spermatozoa, the nucleus exhibited a large, abnormal 'thumbprint'-like concavity at the site of the large vacuole (Fig. 4b and c). This feature was a DAPI-negative area covered by the acrosome and the acrosomal membrane, rather than a hole. Regardless of the large vacuole's position, the acrosome was intact in all 100 vacuolated spermatozoa.

Discussion

Eight years after Bartoov *et al.* (2002) described vacuoles as being nuclear features, their exact nature remains unknown and may depend on the vacuole size and number. Hence, we decided to focus on only one type of vacuole: the single and large vacuole observed in otherwise normal spermatozoa.

The literature data on these vacuoles are divergent because the various studies have examined different types of patients (with differing sperm parameters and DNA fragmentation rates and various degrees of spermatogenesis impairment) and selected different types of spermatozoa (with different types of vacuoles or abnormal or uncharacterized morphologies). In view of this potential methodological and selection bias, we decided to select sperm that were morphologically normal (length range: 4–5 μm; width range: 2.5–3.2 μm) according to both the WHO criteria (length range: 3.7–4.7 μm; width range: 2.5–3.2 μm; WHO, 2009) and Bartoov's criteria (mean length: 4.75 ± 0.28 μm; mean width: 3.28 ± 0.20 μm; Bartoov *et al.* 2002). The 'top' and 'vacuolated' spermatozoa that we examined in detail differed only in terms of the presence or absence of a single, large vacuole. We included patients with various sperm characteristics (various proportions of 'top' and 'vacuolated' spermatozoa, various types of vacuoles, various motility profiles and various sperm concentrations) and thus determined the nature of the large vacuole for various types of sperm.

Our results showed that regardless of the sperm characteristics, the proportion of vacuolated spermatozoa and the vacuole number and size, the large vacuole was always an abnormal, 'thumbprint'-like concavity. In most cases, the presence of a vacuole was associated with a complete or partial failure of chromatin condensation. Although AFM has already been used for human spermatozoa (Joshi *et al.*, 2000, 2001; Mai *et al.*, 2002; Kumar *et al.*, 2005), we described its use here to characterize the large vacuole as a very thin area where the plasma membrane is intact but sunken. Using electron microscopy, Zamboni *et al.* (1971) described sperm nuclear holes that were not bounded by a membrane and were probably areas of uncondensed chromatin. Our data, and particularly the 3D deconvolution microscopy results, show that the large vacuole is an abnormal nuclear concavity covered by the acrosome and the plasma and acrosomal membranes, rather than a hole.

In the sperm nucleus, replacement of histones by protamines results in tightly condensed chromatin. Since aniline blue binds to lysine-rich proteins, the stain can be used as evidence of a lack of histone replacement (Dadoune *et al.*, 1988; Auger *et al.*, 1990; Foresta *et al.*, 1992). In the present study, the non-condensed chromatin rate was significantly higher in vacuolated spermatozoa than in 'top' spermatozoa (36.2 ± 1.9 versus 7.6 ± 1.3%, respectively; $P < 0.0001$). Most of the vacuolated spermatozoa (63.1%, on average) presented non-condensed chromatin (36.2%) or partially non-condensed (26.9%) chromatin. These data are in agreement with other studies (Garolla *et al.*, 2008; Perdrix *et al.*, 2011) and suggest that the presence of a large vacuole reflects a failure of chromatin condensation and subsequent nuclear weakness. Further studies are necessary to establish which persistent histones are present in vacuolated spermatozoa. Another question concerns the origin of the large vacuole in spermatozoa with normal levels of histone replacement. It should be noted that we chose aniline blue staining to evaluate chromatin condensation because it was compatible with TUNEL and FISH assays in a triple-probe procedure. However, aniline blue staining may lack sensitivity and could underestimate the level of chromatin non-condensation (Wong *et al.*, 2008). Furthermore, chromatin packaging is 'matured' in the male genital tract by the establishment of disulphide bonds. The lack of this maturation could lead to insufficient chromatin condensation (Miller *et al.*, 2010) and perhaps the formation of a large vacuole. This lack of chromatin packaging maturation cannot be detected by aniline blue staining. Alternatively, it is possible that these nuclear 'thumbprint'-like vacuoles could be formed by the neighbouring structures pressing on the nucleus during its elongation or maturation, even when the degree of chromatin condensation is not altered.

Nevertheless, most vacuolated spermatozoa present a failure of chromatin condensation. It is known that prior to histone replacement by protamines, the nucleosomes are destabilized [possibly by hyperacetylation (Miller *et al.*, 2010)] and DNA methylation levels rise (Miller *et al.*, 2010). Thus, studies of the epigenetic status of 'vacuolated' spermatozoa may help us to identify the potential epigenetic mechanisms implied in failure of chromatin condensation, such as a lack of DNA methylation or abnormal histone acetylation and methylation.

Whatever the mechanism involved in the genesis of the large vacuole (e.g. the non-replacement of histones, epigenetic modifications of non-replaced histones, the lack of chromatin packaging etc.), the use of high-magnification light microscopy enables the selection of 'top' spermatozoa with normally condensed chromatin. Given the growing evidence that the degree of sperm chromatin condensation at the time of fertilization can influence early and late embryo development (Carrell and Hammoud, 2010), we hypothesize that injection into the oocyte of a spermatozoon with a large vacuole could harm the embryo's ability to develop and implant. Hence, for patients with morphometrically normal spermatozoa and a high degree of non-condensed chromatin, IMSI with non-vacuolated spermatozoa could help increase pregnancy rates. Aniline blue sperm staining would then constitute a screen for patients requiring IMSI.

Sperm DNA fragmentation could also reduce the embryo's ability to implant. In the present study, DNA fragmentation rates were similarly low for both 'top' and 'vacuolated' spermatozoa (0.7 ± 0.4 versus 1.3 ± 0.4%, respectively; $P = 0.25$). These data agree with recent publications (Watanabe *et al.*, 2011). Low DNA fragmentation rates in morphologically normal spermatozoa have already been reported (Gandini *et al.*, 2000; Sati *et al.*, 2008). Other researchers have suggested that the large vacuole is linked to DNA fragmentation but have not always specified the morphology/morphometry of the vacuolated spermatozoa in question; this could introduce methodological bias (Franco *et al.*, 2008; Oliveira *et al.*, 2010). In contrast, Garolla *et al.* (2008) observed a higher DNA-fragmented sperm rate

for vacuolated spermatozoa from patients with severely impaired spermatogenesis. Even though the presence of a large vacuole was not linked to DNA fragmentation in the present study, the use of high-magnification light microscopy enabled us to select 'top' spermatozoa with a low DNA fragmentation rate ($0.7 \pm 0.4\%$, compared with $3.1 \pm 1.4\%$ for spermatozoa obtained after density-gradient selection; $P < 0.005$). These data are in agreement with one of our previous studies (unpublished data) in men with higher-than-average sperm DNA fragmentation rates.

The 'top' and 'vacuolated' spermatozoa studied here did not differ significantly in terms of the aneuploidy rate (1.1 ± 0.5 versus $2.2 \pm 0.7\%$, respectively; $P = 0.25$). These data are in agreement with our previous findings (Chelli *et al.*, 2010). Infertile patients with a normal karyotype have a higher sperm aneuploidy rate than control patients (Shi and Martin, 2001; Tempest and Martin, 2009) but this value does not exceed 2% when three chromosomes are analysed (X, Y and 18, in most studies). In contrast, Perdrix *et al.* (2011) reported extremely high aneuploidy rates for spermatozoa with a large vacuole. Our data prompt us to conclude that the selection of spermatozoa according to the presence of absence of a large vacuole does avoid the selection of aneuploid or euploid spermatozoa. We also noted that 9 out of 15 of the aneuploid spermatozoa exhibited chromatin condensation failure. In agreement with a literature report (Ovari *et al.*, 2010), our data suggest that meiosis abnormalities may affect the later stages of spermiogenesis in general and chromatin condensation in particular.

In conclusion, the large vacuole is a nuclear thumbprint-like concavity linked to failure of sperm chromatin condensation. This concavity is covered by the acrosome, the acrosomal membrane and the plasma membrane. The investigation of spermatozoa with large head vacuoles may be useful for understanding epigenetic events involved in spermiogenesis in general and chromatin condensation in particular. Our results argue in favour of a new indication for IMSI in patients with morphometrically normal spermatozoa with non-condensed chromatin. However, further studies are needed to understand the mechanisms involved in the genesis of these vacuoles. One can speculate that a nuclear 'thumbprint'-like vacuole mirror the spermatozoon's 'birth' and 'maturation' and that the spermatozoon may bear the mark of the (epigenetic) events that it has experienced.

Authors' roles

F.B. designed and performed experiments, performed the statistical analysis and drafted the manuscript. F.F. critically revised the manuscript. J.M.P., D.S. and C.T. performed atomic force microscopy and 3D deconvolution microscopy analyses. M.B. helped to design the study. M.B. recruited patients. F.V. evaluated the experiments' feasibility and critically revised the manuscript critically. J.S. and M.A. designed the study, evaluated the experiments' feasibility and critically revised the manuscript. All authors have approved the final manuscript.

References

Antinori M, Licata E, Dani G, Cerusico F, Versaci C, d'Angelo D, Antinori S. Intracytoplasmic morphologically selected sperm injection: a prospective randomized trial. *Reprod Biomed online* 2008;**16**:835–841.

Auger J, Mesbah M, Huber C, Dadoune JP. Aniline blue staining as a marker of sperm chromatin defects associated with different semen characteristics discriminates between proven fertile and suspected infertile men. *Int J Androl* 1990;**13**:452–462.

Bartoov B, Berkovitz A, Eltes F, Kogosowski A, Menezo Y, Barak Y. Real-time fine morphology of motile human sperm cells is associated with IVF-ICSI outcome. *J Androl* 2002;**23**:1–8.

Bartoov B, Berkovitz A, Eltes F, Kogosovsky A, Yagoda A, Lederman H, Artzi S, Gross M, Barak Y. Pregnancy rates are higher with intracytoplasmic morphologically selected sperm injection than with conventional intracytoplasmic injection. *Fertil Steril* 2003;**80**:1413–1419.

Berkovitz A, Eltes F, Yaari S, Katz N, Barr I, Fishman A, Bartoov B. The morphological normalcy of the sperm nucleus and pregnancy rate of intracytoplasmic injection with morphologically selected sperm. *Hum Reprod* 2005;**20**:185–190.

Berkovitz A, Eltes F, Ellenbogen A, Peer S, Feldberg D, Bartoov B. Does the presence of nuclear vacuoles in human sperm selected for ICSI affect pregnancy outcome? *Hum Reprod* 2006;**21**:1787–1790.

Biggs DS. 3D deconvolution microscopy. *Curr Protoc Cytom* 2010;**12**:1–20.

Carrell DT, Hammoud SS. The human sperm epigenome and its potential role in embryonic development. *Mol Hum Reprod* 2010;**16**:37–47.

Cassuto NG, Bouret D, Plouchart JM, Jellad S, Vanderzwalmen P, Balet R, Larue L, Barak Y. A new real-time morphology classification for human spermatozoa: a link for fertilization and improved embryo quality. *Fertil Steril* 2009;**92**:1616–1625.

Chelli MH, Albert M, Ray PF, Guthauser B, Izard V, Hammoud I, Selva J, Vialard F. Can intracytoplasmic morphologically selected sperm injection be used to select normal-sized sperm heads in infertile patients with macrocephalic sperm head syndrome? *Fertil Steril* 2010;**93**:1347.

Dadoune JP, Mayaux MJ, Guihard-Moscato ML. Correlation between defects in chromatin condensation of human spermatozoa stained by aniline blue and semen characteristics. *Andrologia* 1988;**20**:211–217.

De Vos A, Van de Velde H, Joris H, Verheyen G, Devroey P, Van Steirteghem A. Influence of individual sperm morphology on fertilization, embryo morphology, and pregnancy outcome of intracytoplasmic sperm injection. *Fertil Steril* 2003;**79**:42–48.

Foresta C, Zorzi M, Rossato M, Varotto A. Sperm nuclear instability and staining with aniline blue: abnormal persistence of histones in spermatozoa in infertile men. *Int J Androl* 1992;**15**:330–337.

Frainais C, Vialard F, Rougier N, Aegerther P, Damond F, Ayel JP, Yazbeck C, Hazout A, Selva J. Impact of freezing/thawing technique on sperm DNA integrity in HIV-1 patients. *J Assist Reprod Genet* 2010;**27**:415–421.

Franco JG, Baruffi RL, Mauri AL, Petersen CG, Oliveira JB, Vagnini L. Significance of large nuclear vacuoles in human spermatozoa: implications for ICSI. *Reprod Biomed Online* 2008;**17**:42–45.

Gandini L, Lombardo F, Paoli D, Caponecchia L, Familiari G, Verlengia C, Dondero F, Lenzi A. Study of apoptotic DNA fragmentation in human spermatozoa. *Hum Reprod* 2000;**15**:830–839.

Garolla A, Fortini D, Menegazzo M, De Toni L, Nicoletti V, Moretti A, Selice R, Engl B, Foresta C. High-power microscopy for selecting spermatozoa for ICSI by physiological status. *Reprod Biomed Online* 2008;**17**:610–616.

Hazout A, Dumont-Hassan M, Junca AM, Cohen Bacrie P, Tesarik J. High-magnification ICSI overcomes paternal effect resistant to conventional ICSI. *Reprod Biomed Online* 2006;**12**:19–25.

Joshi N, Medina H, Colasante C, Osuna A. Ultrastructural investigation of human spermatozoon by using atomic force microscope. *Arch Androl* 2000;**44**:51–57.

Joshi N, Medina H, Cruz I, Osuna J. Determination of the ultrastructural pathology of human sperm by atomic force microscopy. *Fertil Steril* 2001;**75**:961–965.

Kacem O, Sifer C, Barraud-Lange V, Ducot B, De Ziegler D, Poirot C, Wolf J. Sperm nuclear vacuoles, as assessed by motile sperm organellar morphological examination, are mostly of acrosomal origin. *Reprod Biomed Online* 2010;**20**:132–137.

Kruger TF, Acosta AA, Simmons KF, Swanson RJ, Matta JF, Veeck LL, Morshedi M, Brugo S. New method of evaluating sperm morphology with predictive value for human *in vitro* fertilization. *Urology* 1987;**30**:248–251.

Kumar S, Chaudhury K, Sen P, Guha SK. Atomic force microscopy: a powerful tool for high-resolution imaging of spermatozoa. *J Nanobiotechnol* 2005;**27**:3–9.

Loutradi KE, Tarlatzis BC, Goulis DG, Zepiridis L, Pagou T, Chatziioannou E, Grimbizis GF, Papadimas I, Bontis I. The effects of sperm quality on embryo development after intracytoplasmic sperm injection. *J Assist Reprod Genet* 2006;**23**:69–74.

Mai A, Weerachatyanukul W, Tomietto M, Wayner DD, Wells G, Balhorn R, Leader A, Cyr JL, Tanphaichitr N. Use of atomic force microscopy for morphological and morphometric analyses of acrosome intact and acrosome-reacted human sperm. *Mol Reprod Dev* 2002;**63**:471–479.

Miller D, Brinkworth M, Iles D. Paternal DNA packaging in spermatozoa: more than the sum of its parts? DNA, histones, protamines and epigenetics. *Reproduction* 2010;**139**:287–301.

Morozumi K, Yanagimachi R. Incorporation of the acrosome into the oocyte during intracytoplasmic sperm injection could be potentially hazardous to embryo development. *Proc Natl Acad Sci USA* 2005;**102**:14209–14214.

Oliveira JB, Massaro FC, Baruffi RL, Mauri AL, Petersen CG, Silva LF, Vagnini LD, Franco JG. Correlation between semen analysis by motile sperm organelle morphology examination and sperm DNA damages. *Fertil Steril* 2010;**94**:1937–1940.

Ovari L, Sati L, Stronk J, Borsos A, Ward DC, Huszar G. Double probing individual human spermatozoa: aniline blue staining for persistent histones and fluorescence in situ hybridization for aneuploidies. *Fertil Steril* 2010;**93**:2255–2261.

Palermo G, Joris H, Devroey P, Van Steirteghem AC. Pregnancies after intracytoplasmic injection of single spermatozoon into an oocyte. *Lancet* 1992;**340**:17–18.

Perdrix A, Travers A, Chelli MH, Escalier D, Do Rego JL, Milazzo JP, Mousset-Siméon N, Macé B, Rives N. Assessment of acrosome and nuclear abnormalities in human spermatozoa with large vacuoles. *Hum Reprod* 2011;**26**:47–58.

Sati L, Ovari L, Benett D, Simon SD, Demir R, Huszar G. Double probing of human spermatozoa for persistent histones, surplus cytoplasm, apoptosis and DNA fragmentation. *Reprod Biomed Online* 2008; **16**:570–579.

Shi Q, Martin RH. Aneuploidy in human spermatozoa: FISH analysis in men with constitutional chromosomal abnormalities, and in infertile men. *Reproduction* 2001;**121**:655–666.

Tempest HG, Martin RH. Cytogenetic risks in chromosomally normal infertile men. *Curr Opin Obstet Gynecol* 2009;**21**:223–227.

Vanderzwalmen P, Hiemer A, Rubner P, Bach M, Neyer A, Stecher A, Uher P, Zintz M, Lejeune B, Vanderzwalmen S *et al.* Blastocyst development after sperm selection at high magnification is associated with size and number of nuclear vacuoles. *Reprod Biomed Online* 2008; **17**:617–627.

Vialard F, Hammoud I, Molina-Gomes D, Wainer R, Bergere M, Albert M, Bailly M, de Mazancourt P, Selva J. Gamete cytogenetic study in couples with implantation failure: aneuploidy rate is increased in both couple members. *J Assist Reprod Genet* 2008;**25**:539–545.

Watanabe S, Tanaka A, Fujii S, Mizunuma H, Fukui A, Fukuhara R, Nakamura R, Yamada K, Tanaka I, Awata S *et al.* An investigation of the potential effect of vacuoles in human sperm on DNA damage using a chromosome assay and the TUNEL assay. *Hum Reprod* 2011 (in press).

Wong A, Chuan SS, Patton WC, Jacobson JD, Corselli J, Chan PJ. Addition of eosin to the aniline blue assay to enhance detection of immature sperm histones. *Fertil Steril* 2008;**90**:1999–2002.

World Health Organization. *WHO Laboratory Manual for the Examination and Processing of Human Semen*, 5th edn. Cambridge, UK: Cambridge University Press, 2009.

Zamboni L, Zemjanis R, Stefanini M. The fine structure of monkey and human spermatozoa. *Anat Rec* 1971;**169**:129–53.